Proceedings of the 10th World Congress on Momentum, Heat and Mass Transfer (MHMT 2025)
Barcelona, Spain - April, 2025
Paper No. CSP 127
DOI: 10.11159/csp25.127

Advancing Industrial Smokeless Flaring: Experimental Study into a Swirl Air-Assist Burner

Jianfeng Hou[1], Jan Werner[2], A. Michael Birk[1]
[1] Department of Mechanical and Materials Engineering, Queen's University
130 Stuart St, Kingston, ON K7L 2V9, Canada
jianfeng.hou@queensu.ca; birka@queensu.ca
[2] Federal Institute for Materials Research and Testing (BAM)
12489 Berlin, Germany
jan.werner@bam.de

Abstract **-** The performance of a prototype swirl air-assist burner, designed to suppress flame thermal radiation and improve flame stability in crosswinds for industrial smokeless flaring, was experimentally investigated. The burner features a central swirl core shaped like a diffuser, equipped with tangential swirl blades to promote mixing between fuel and air. It was tested using vapour propane at assist-air-to-fuel ratios (AAFRs) ranging from about 29 to 80, which gradually led to the formation of a central recirculation region. Visible flame characteristics were recorded with a video camera, while thermal radiation properties-including emissive power and emissivity-were measured using an infrared camera. Increasing the AAFR reduced the flame's height-to-width ratio, thereby enhancing flame stability under crosswind conditions. Smoke production also diminished, transitioning from a heavily smoky flame to a cleaner one. As the AAFR increased from 0 to its maximum value, the flame area (m^2) and emissive power (W/m^2) decreased by 69% and 24%, respectively. Overall, the experimental results confirm the suitability of this swirl air-assist burner design for industrial smokeless flaring, demonstrating improved performance in stabilizing the flame under crosswind conditions.

Keywords**:** Smokeless flaring, Swirl air-assist burner, Thermal radiation, Soot production, Large-scale field tests

1. Introduction

Efforts to mitigate thermal radiation levels and soot production in flare systems are advancing through the incorporation of various design enhancements. One effective strategy involves introducing a separate assisting fluid, such as air, at the base of the flame. This technique enhances fuel mixing, and adds momentum to the flare discharge, thereby entraining more combustion air from the surrounding environment [1]. Flame stability in crosswind also needs to be achieved mainly to avoid significant combustion efficiency reduction in high crosswind condition [2]. A stable flame would also help evenly distribute radiative flux to the surrounding, avoiding extreme heat concentration towards one direction.

Imparting a swirl to the assist-air can create a rotational airflow, producing a wider, shorter flame [3] that potentially reduces thermal radiation more effectively and stabilizes the flame in crosswinds. Designing swirling air-assisted flare burners requires reliable large-scale experiments to understand flame properties. However, large-scale fire tests are exceedingly costly and limited to a few experimental facilities globally. Although a few large-scale turbulent jet flames exist (e.g. Palacios and Casal [4]; Zhang et al. [5]), they are inadequate for inferring the characteristics of swirling air-assisted flames. Studies on confined swirl burners are common due to the widespread use of gaseous fuel burners and gas turbines, such as Subash et al. [6]. But investigations of unconfined swirl combustors, particularly at large scales, remain scarce.

This work is driven by the objective to experimentally investigate the capabilities of a prototype swirl burner in reducing thermal radiation levels, decreasing soot emissions, and stabilizing flames in crosswinds, facilitating further advancements in burner design. In the present manuscript, the design of the burner is first briefly introduced, followed by the discussion of detailed experimental setups. The improvements in flame properties are demonstrated by comparing the flames at different assist-air-to-fuel ratio (AAFR) in mass.

2. Methodology

2.1. Design of the burner

A prototype air-assisted swirl burner mainly containing a cylindrical air box, a diffusing swirl core, four tangential air inlets to be connected to transition ducts was developed, see Fig. 1. The diffusing swirl core is in the shape of a diffuser to accommodate large flow rates of fuel and air similar as in real flare tip operating condition. It has eight tangential swirl blades to promote swirling motions of the assist-air. The fuel enters from the burner bottom via fuel lines, while the assist-air enters from the end of the transition ducts. Transition ducts can either be two or four, depending on the air flow rates needed.

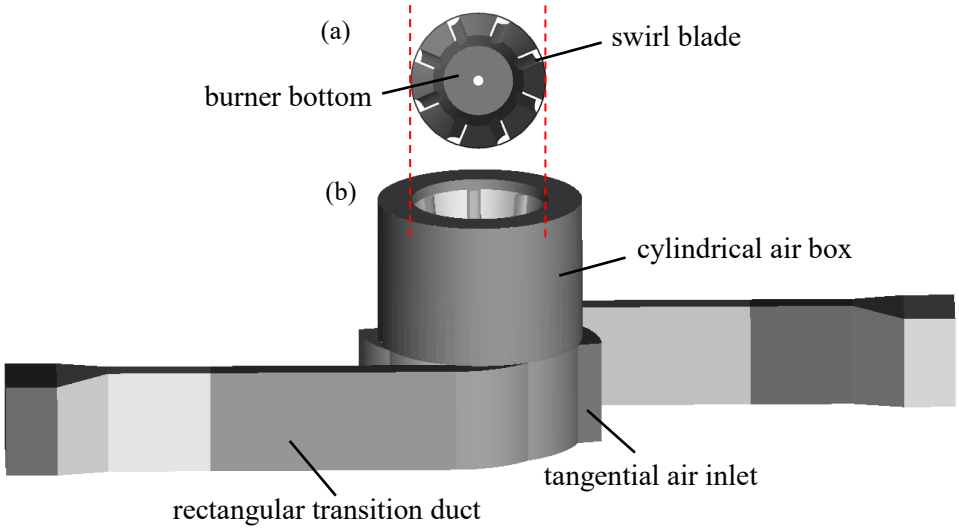

Fig. 1: Geometry of the prototype swirl burner with two transition ducts (a) top view of the diffusing swirl core and burner bottom, (b) full geometry of the burner.

2.2. Experimental setup

The experiments were conducted at the technical safety test site of Federal Institute for Materials Research and Testing (BAM) in Berlin, Germany.

The swirl burner was placed on concrete blocks and the setup is shown in Fig. 2. The bottom of the burner was connected to a 25 mm fuel nozzle for vapour propane supply. The proposed high mass flow rates of the vapour propane were not achieved due to some restrictions on the test site, therefore the mass flow rates $\dot{m}_{\mathrm{fuel}}$ were selected to stay around 2.4 and 3.7 kg/min. Because of the reduced fuel flow rates, the two powerful centrifugal fans (DCMR-1650-2T Motor 11kW) delivered excess air, resulting in high AAFRs and the appearance of recirculation regions near the burner outlet.

Ten K-type thermocouples, each capable of measuring temperatures from –270 °C to 1372 °C, were suspended from a mast above the burner to record flame temperatures at two axial and five spanwise positions (see Fig. 2). Each thermocouple was placed inside a short metal tube to reduce thermal radiation errors and to better capture the actual flame temperature. In both measurement rows, the thermocouples in the middle were positioned along the burner's vertical centerline.

An infrared camera, VarioCAM High Definition (resolution 1024 × 768, spectrum range 7.5–14 µm, 15° lens and selected temperature range 250-1200 °C), and a video camera were located 20 m south of the swirl burner. The former recorded flame thermal radiation properties by assuming the flame as blackbody and the latter captured images of the visible flame and the smoke. Both cameras recorded at 30 Hz.

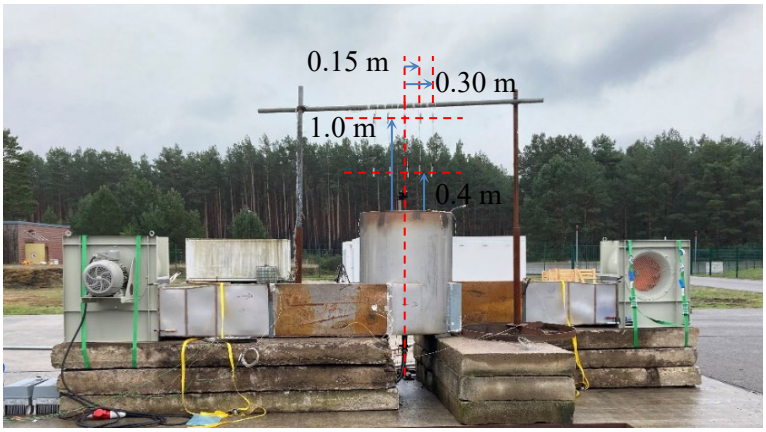

Fig. 2: Air assisted swirl burner experiment setup. The burner was lifted and the bottom inlet was connected to the fuel pipe and nozzle; two centrifugal fans supplied air through the transition ducts. Video camera and infrared camera not included in this figure.

The unassisted flare setup was also considered as a baseline performance to compare with the air-assisted swirl burner. The setup is called open nozzle condition, see Fig. 3. The same measurement instruments were employed as the swirl burner setup but placed at different locations, such as the lower thermocouple row was 0.8 m from the nozzle top, the upper row was 1.4 m from the nozzle top, and the video camera and the infrared camera were located 13 m south of the open nozzle.

Fig. 3: Baseline open nozzle experiment setup. Video camera and infrared camera were located to the south of the open nozzle.

Two series of subsonic tests were conducted featuring the swirl burner and the open nozzle, corresponding to 2.4 and 3.7 kg/min fuel flow rates and different assist-air level, see Table 1. Note that the assisted air rates were not measured directly or precisely but were estimated based on tangential velocity measurements at a location near the diffusing swirl core. The prevailing wind was from the southeast at approximately 2 m/s during the tests. Flame measurements were taken when the flames under the new test condition reached steady state.

Table 1: Summary of test conditions of the air-assisted swirl burner and the open nozzle setup with vapour propane.

Test No.	$\dot{m}_{\text{fuel}}$/kgmin^{-1}	Estimated $\dot{m}_{\text{assist-air}}$ per blower/ kgmin^{-1}	Estimated AAFR
Series 1 Swirl burner			
1	2.5	52.8	42
2	2.4	60.0	50
3	2.4	78.0	65
4	2.4	96.0	80
5	3.7	52.8	29
6	3.7	60.0	32
7	3.8	78.0	41
8	3.9	96.0	49
Series 2 Open nozzle			
9	2.4	-	-
10	3.7	-	-

2.3. Analysis method

The thermal radiation properties of the flame were analyzed using an iterative emissivity method [7]. As noted earlier, the infrared camera treated the flame as a blackbody. By iteratively assigning an initial emissivity value, the method matched the blackbody's emissive power to the actual flame's emissive power from regions at a predefined boundary temperature over the spectrum range of the camera. This approach enabled the estimation of the flame's emissive power E[W/m^2], and its emissivity ε. A boundary temperature of 800 K was chosen based on the observation by Palacios and Casal [4] that the visible propane flame size closely matched the $\geqslant$800 K regions observed in infrared flame images.

3. Results

Fig. 4 presents images of the flame above the burner exit for various combinations of fuel and assist air flow rates.

At $\dot{m}_{\text{fuel}}$ = 3.7 kg/min, lowest AAFR conditions yielded flames resembling a cylindrical shape, much like an unassisted flare, as shown in Fig. 4 (a)-(c). These flames exhibited the highest luminosity due to excess soot formation caused by limited oxygen in the combustion zone. As the AAFR increased at the same fuel flow rate, see Fig. 4 (d), the recirculation regions near the burner outlet formed and therefore suppressed the flame in height but stretched the flame width. The flame transitioned into a more spherical shape, demonstrating excellent wind stability. Meanwhile, soot levels decreased noticeably, resulting in much cleaner flames and reflecting improved combustion efficiency.

At $\dot{m}_{\text{fuel}}$ = 2.4 kg/min, similar reductions in flame height and soot production were observed with the increase of AAFR, see Fig. 4 (e)-(h). Moreover, the maximum AAFR value produced the flame with an obvious empty region at the centre, with flame swirling only around the burner outer circle, see Fig. 4 (h).

It is therefore concluded that the prototype swirl burner could produce three types of flames, from low to high AAFR, (1) cylindrical and smoky, (2) spherical and smokeless, and (3) center-void spherical and smokeless. A more detailed analysis on thermal radiation properties in Fig. 5 provides more insights on the best operating AAFR range for the current prototype swirl burner.

(a) AAFR = 29 (b) AAFR = 32 (c) AAFR = 41 (d) AAFR = 49

(e) AAFR = 42 (f) AAFR = 50 (g) AAFR = 65 (h) AAFR = 80

Fig. 4: Visible propane flames at different AAFR (a)-(d) $\dot{m}_{\text{fuel}}$ = 2.4 kg/min, (e)-(h) $\dot{m}_{\text{fuel}}$ = 3.7 kg/min.

Fig. 5 (a) suggests that all flames within the 800K boundary, $A_{800\text{K}}$ from the burner had smaller flame area compared to the open, unassisted flare. At $\dot{m}_{\text{fuel}}$ = 2.4 kg/min, the $A_{800\text{K}}$ reduced from 1.8 to 1.1 m^2 at AAFR = 42 and 80, respectively, representing a 39% change. When $\dot{m}_{\text{fuel}}$ = 3.7 kg/min, the flame size increased correspondingly compared to low fuel flow rate situations at similar AAFR. The $A_{800\text{K}}$ decreased by 40% when increasing the AAFR from 29 to 49. However, when 20 < AAFR < 40, the flame area even experienced an increase when supplying more assist air, indicating an unsteady operating range.

The flame emissivities calculated within the 800K boundary are given in Fig. 5 (b). For open flares, emissivities of about 0.4 were observed, closely matched with ~0.4 measured over propane flames in similar conditions as in the current study by Palacios et al. [8] and Lowesmith et al. [9]. For both fuel flow rates, flames at lower AAFR had higher emissivities around 0.5, due to more soot production and increased mean beam length for wider flames. For smokeless flames at high AAFR, the higher emissivities around 0.4 could be ascribed to the even larger mean beam length because of the spherical flames. A decrease in fuel flow rate and an increase in AAFR would both lead to reduction in emissivity.

The emissive power flames emitted per area is provided in Fig. 5 (c). At $\dot{m}_{\text{fuel}}$ = 3.7 kg/min, the burner flames exhibit no improvement over open flames due to increased emissivity as a result of reduced combustion efficiency in the burner. Not enough air and fuel mixing was achieved even though the air supply was excess, suggesting the necessity for better diffusing swirl core design. When $\dot{m}_{\text{fuel}}$ = 2.4 kg/min, only at very high AAFR, the emissive power of swirling flames was finally brought down, but at the cost of sacrificing combustion efficiency.

Considering about the total emissive power, see Fig. 5 (d), the swirl burner flames benefiting from reduced flame area showed improvement over open flames. A 31% and an 18% reduction were achieved when increasing the AAFR from 0 to about 41, for low and high fuel flow rates, respectively.

To balance the AAFR and combustion efficiency, the current prototype swirl burner could be operated right above AAFR = 40. At this AAFR range, shape change to stable spherical flame in crosswind has fulfilled, significant reductions in soot production, flame area, and emissive power can also realize. However, further improvement in swirl core design is still relevant as the AAFR is still very high compared to many flaring practices.

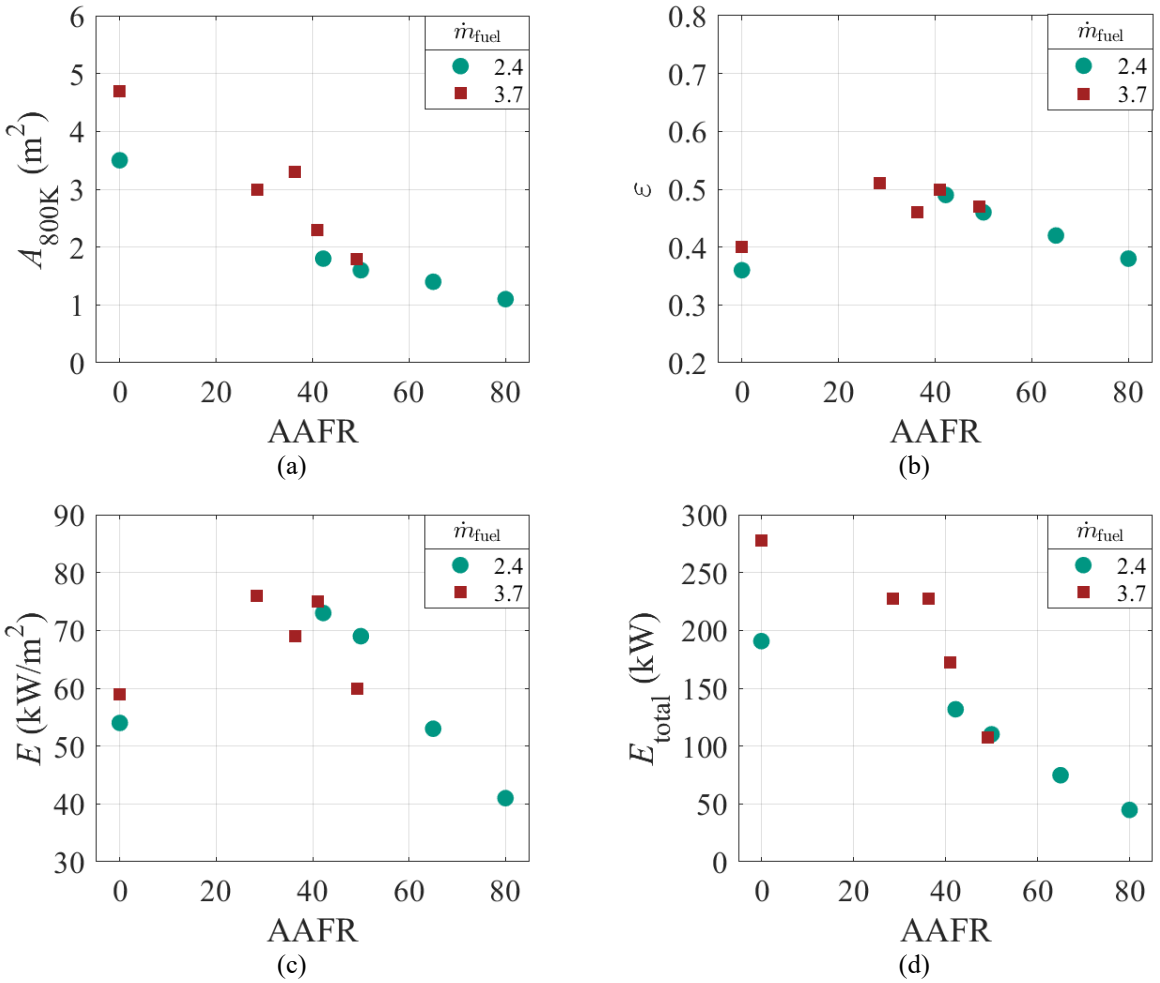

Fig. 5: Comparison of thermal radiation related results from infrared images recorded by the infrared camera (a) flame area within 800 K contour, (b) emissivity, (c) emissive power, (d) total emissive power (figure (b) and (d) are derived from author's work in [7])

4. Conclusion

A prototype swirl air-assist burner was tested using vapour propane across a broad range of assist-air-to-fuel ratios (AAFRs). As the AAFR increased, the flame transitioned from a cylindrical, smoky configuration to a more spherical, smokeless one, primarily due to enhanced combustion efficiency and the development of a central recirculation zone. This transformation significantly improved flame stability under crosswind conditions. In addition, higher AAFRs led to noticeable reductions in flame area and emissive power, approximately 49% and 31% decreases, respectively, when comparing an AAFR of 0 to 42 at the tested low fuel flow rate. Based on these findings, an AAFR above 40 is recommended for optimal performance with the current burner design. Further refinements to the swirl core design may be necessary to achieve even better results.

Acknowledgements

The authors gratefully acknowledge the financial support provided by Davis Engineering Ltd. and the Natural Sciences and Engineering Research Council of Canada (NSERC) through the Collaborative Research Development grant. We also extend our sincere thanks to Professor Frank Otremba for granting access to the Bundesanstalt für

Materialforschung und -prüfung (BAM, Federal Institute for Materials Research and Testing) Division 3.2 in Germany, as well as to Dr. Tobias Gleim of BAM Division 3.3 and the entire team at BAM Division 3.2 for their invaluable assistance during the measurement campaign.

References

[1] T. Poinsot and D. Veynante, *Theoretical and Numerical Combustion*. Bordeaux, France: R. T. Edwards, 2012.
[2] M. R. Johnson and L. W. Kostiuk, "A parametric model for the efficiency of a flare in crosswind," *Proc. Combust. Inst.*, vol. 29, no. 2, pp. 1943-1950, 2002.
[3] R. H. Chen and J. F. Driscoll, "The role of the recirculation vortex in improving fuel-air mixing within swirling flames," *Proc. Symp. Combust.*, vol. 22, pp. 531-540, 1989.
[4] A. Palacios and J. Casal Fàbrega, "The behaviour of vertical jet fires under sonic and subsonic regimes," *Chem. Eng. Trans.*, vol. 19, pp. 183-188, 2010.
[5] B. Zhang, Y. Liu, D. Laboureur, and M. S. Mannan, "Experimental study on propane jet fire hazards: thermal radiation," *Ind. Eng. Chem. Res.*, vol. 54, no. 37, pp. 9251-9256, 2015.
[6] A. A. Subash, S. Yu, X. Liu, M. Bertsch, R. Z. Szasz, Z. Li, X. S. Bai, M. Aldén, and D. Lörstad, "Flame investigations of a laboratory-scale CECOST swirl burner at atmospheric pressure conditions," *Fuel*, vol. 279, art. no. 11842, 2020.
[7] J. Hou, "Advancing industrial smokeless flaring: experimental and computational studies into swirl air-assist burners," Ph.D. dissertation, Dept. Mech. Eng., Queen's Univ., Kingston, ON, 2024.
[8] A. Palacios, M. Muñoz, R. M. Darbra, and J. Casal, "Thermal radiation from vertical jet fires," *Fire Saf. J.*, vol. 51, pp. 93-101, 2012.
[9] B. J. Lowesmith, G. Hankinson, M. R. Acton, and G. Chamberlain, "An overview of the nature of hydrocarbon jet fire hazards in the oil and gas industry and a simplified approach to assessing the hazards," *Process Saf. Environ. Prot.*, vol. 85, no. 3, pp. 207-220, 2007.